PCCP

ROYAL SOCIETY OF CHEMISTRY

PAPER

View Article Online
View Journal | View Issue

Cite this: *Phys. Chem. Chem. Phys.*, 2021, **23**, 9476

Hidden polymorphism of $FAPbI_3$ discovered by Raman spectroscopy†

Josefa Ibaceta-Jaña, *[a] Ruslan Muydinov, *[a] Pamela Rosado,[b] Sri Hari Bharath Vinoth Kumar,[a] Rene Gunder,[c] Axel Hoffmann,[b] Bernd Szyszka[a] and Markus R. Wagner[b]

Formamidinium lead iodide ($FAPbI_3$) can be used in its cubic, black form as a light absorber material in single-junction solar cells. It has a band-gap (1.5 eV) close to the maximum of the Shockley–Queisser limit, and reveals a high absorption coefficient. Its high thermal stability up to 320 °C has also a downside, which is the instability of the photo-active form at room temperature (RT). Thus, the black α-phase transforms at RT with time into a yellow non-photo-active δ-phase. The black phase can be recovered by annealing of the yellow state. In this work, a polymorphism of the α-phase at room temperature was found: as-synthesized (α_i), degraded (α_δ) and thermally recovered (α_{rec}). They differ in the Raman spectra and PL signal, but not in the XRD patterns. Using temperature-dependent Raman spectroscopy, we identified a structural change in the α_i-polymorph at *ca.* 110 °C. Above 110 °C, the $FAPbI_3$ structure has undoubtedly cubic $Pm\bar{3}m$ symmetry (high-temperature phase: α_{HT}). Below that temperature, the α_i-phase was suggested to have a distorted perovskite structure with $Im\bar{3}$ symmetry. Thermally recovered $FAPbI_3$ (α_{rec}) also demonstrated the structural transition to α_{HT} at the same temperature (*ca.* 110 °C) during its heating. The understanding of hybrid perovskites may bring additional assets in the development of new and stable structures.

Received 8th January 2021,
Accepted 1st March 2021

DOI: 10.1039/d1cp00102g

rsc.li/pccp

1 Introduction

Hybrid perovskites have drawn genuine attention of scientists in the past several years. Along with the studies on their applications as prospective semiconductors, particular attention was paid to understanding the phenomenon of so-called defect tolerance and stability issues.[1] The dynamics of the relatively rigid network of PbI_6 octahedra as well as the rotational activity of the organic cation can give basic answers to those questions.[2,3] The formamidinium cation ($FA^+ = NH_2–C–NH_2^+$) has replaced the methylammonium cation ($MA^+ = CH_3NH_3^+$) in hybrid perovskite semiconductors used in the study of solar cells.[4] $FAPbI_3$ has a narrower bandgap than $MAPbI_3$ (1.5 eV *vs.* 1.59 eV), closer to the Shockley–Queisser limit. Furthermore, $FAPbI_3$ decomposes at a much higher temperature (320 °C *vs.* 275 °C).[5–8] There are two known polymorphs of $FAPbI_3$ at room temperature (RT = 20 °C): photo-active (black) α and non-photo-active (yellow) δ. The first one crystallizes from γ-butyrolactone (GBL) solution at 110 °C, remaining stable in the GBL-solution at temperatures above 60 °C.[9,10] At RT, the α-form transforms into the δ-form due to the structural instability attributed to internal stress.[1] This transformation occurs in about 1 day when single crystals are stored in ambient air with a relative humidity of 55–57% and up to 10 days when they are stored in a vacuum or inert gas.[7,9] Polycrystal α-$FAPbI_3$ can be recovered from the δ crystal *via* annealing, which in turn retards the α → δ phase-transition up to 20 to 30 days.[10–14] Differential scanning calorimetry performed on δ-$FAPbI_3$ showed an endothermic peak at 160 °C for the powder and at 185 °C for single crystals, which is attributed to the reverse δ → α phase-transition.[7,15] Chemical decomposition of δ-$FAPbI_3$ single crystals takes place at higher temperatures: HI decomposes around 320–360 °C, while FA^+ around 375–420 °C.[7]

The structure of the δ-phase is accepted as hexagonal $P6_3mc$.[10] On the contrary, the structure of the α-phase is still a matter of scientific debate in the literature.

Recent studies based on X-ray diffraction (XRD) and powder neutron diffraction define thermally recovered $FAPbI_3$ (α-phase) as a cubic perovskite with $Pm\bar{3}m$ symmetry,[12,16] refuting the structure previously assigned as trigonal P3.[10] The discussion arises when the structural instability of the α-phase and the structure of the

[a] *Technology for Thin Film devices, Technische Universitat Berlin, Einsteinufer 25, 10587 Berlin, Germany. E-mail: ibacetajana@campus.tu-berlin.de, ruslan.muydinov@tu-berlin.de*
[b] *Institute of Solid State Physics, Technische Universitat Berlin, Hardenberg st. 36, 10623 Berlin, Germany*
[c] *Department Structure and Dynamics of Energy Materials (EM-ASD), Helmholtz-Zentrum Berlin für Materialien und Energie GmbH, Hahn-Meitner-Platz 1, D-14109 Berlin, Germany*

† Electronic supplementary information (ESI) available: Additional Raman, PL and XRD measurements of $FAPbI_3$. See DOI: 10.1039/d1cp00102g

molecular cation are considered. Other characteristics that lack explanation if the cubic $Pm\bar{3}m$ symmetry is considered are listed in the following. First, the Goldschmidt tolerance factor of $FAPbI_3$ is equal to 1.008, which predicts structural stability for perovskites. Also, the combination with cubic $Pm\bar{3}m$ $FAPbBr_3$ presents an instability region from 30 to 50% of $FAPbBr_3$, which is unexpected in a mixture of materials possessing the same space group.[17] Density functional theory (DFT) calculations give a band-gap energy 0.2 eV lower than that experimentally observed if cubic $Pm\bar{3}m$ is considered.[18] A more precise result (+0.05) is obtained for a relaxed tetragonal structure with head-to-tail cation organization. Carignano *et al.* studied octahedral distortions in $FAPbI_3$ using molecular dynamics simulations and group theory.[19,20] These results showed that the cubic $Pm\bar{3}m$ structure adequately represents the material at 177 °C due to the harmonicity of the vibrations, but at 27 °C the distortion of the structure can be better described by the cubic symmetry $Im\bar{3}$. In this case, the body centered cell is eight-times larger than the primitive one.

As presented above, such distorted cubic structures as $Im\bar{3}$ are considered in the literature as relevant for $FAPbI_3$;[19] however, there is no direct experimental proof yet. Additionally, the fresh-synthesized material and the thermally recovered one are not usually differentiated, even though there is a clear disparity in their structural stability. We also point out that the structural instability has not been explored in terms of distortion of the $FAPbI_3$ structure.

In this work, we expand the knowledge about the polymorphism of $FAPbI_3$ at RT. For this, we characterized single crystals by Raman spectroscopy and supported our findings with XRD and photoluminescence (PL). We identify 4 polymorphs: 3 photo-active α (fresh-synthesized, degraded, and thermally recovered) and one non-photo-active δ (degraded). To support these analyses, time or temporally dependent XRD and Raman-spectroscopy measurements were undertaken to characterise the transition from the fresh-synthesized state (RT) to the high temperature state (200 °C), then the transition from the fresh-synthesized state to the degraded state (after 1 day), and the recovery of the degraded state (RT) *via* sequential annealing up to 180 °C.

2 Methods

2.1 Sample preparation

Single crystals (SCs) of the $FAPbI_3$ compound were synthesized following the modified inverse temperature crystallization method reported by Saidaminov *et al.*[9] 1 M of precursors FAI (DyeSol) and PbI_2 (99.99% TCI) was dissolved in 1 ml of GBL at room temperature (RT = 20 °C) in a controlled N_2 atmosphere (H_2O < 1 ppm, O_2 < 10 ppm). The solubility was increased by placing the vials over a preheated hot plate at 60 °C for at least 1 h. The solution was then filtered through a 0.2 μm polytetrafluoroethylene syringe filter, poured into a 10 ml vial and placed over a preheated hot plate at 90 °C. The temperature was elevated in steps of 5 °C h^{-1} up to 115 °C and kept for 3 h to increase the crystal size. After that, the crystals were wiped with filter paper and dried with N_2 gas flux. Powder samples were obtained by grinding of single crystals in an agate mortar.

2.2 Experimental methods

Raman spectroscopy was performed on a high-resolution LabRAM HR800 spectrometer (Horiba). The equipment has an ultra-low frequency (ULF) unit that allows measuring from 10 cm^{-1} for an excitation wavelength of 633 nm. Spectra were recorded with a mesh of 600 and 1800 lines per mm. The laser beam was focused using 50×/0.75 and 100×/0.90 microscope objectives. The power was maintained within a range of 70 to 90 μW, considering a restriction of 1 mW for the selected wavelength to avoid degradation by the laser.[3] The reproducibility of the measurements was probed through the analysis of several samples, whose normalized Raman spectra are presented in Fig. S1 (ESI†). The Raman spectra of the polymorphs are invariant in terms of the position of the Raman modes, supporting our attribution. The difference in intensity is related to the instrument adjustment. The spectrum of PbI_2 resulting from measuring $FAPbI_3$ with a power higher than 1 mW is presented in Fig. S2 (ESI†). Supportive PL measurements are presented in Fig. S3–S5 (ESI†). XRD patterns were acquired using Cu Kα radiation on a D8 Discover diffractometer from Bruker. A high resolution model of the LYNXEYE XE-T detector in combination with 2.5° axial parallel-slit collimators and 0.6 mm slits from the primary and secondary beam sides was used. Measurements were performed in a Bragg–Brentano geometry with a 0.02° step size and 2 s step time. Differently annealed thin films, powder and small as-synthesized single crystals (*ca.* 0.5 mm) were measured in ambient air. These measurements were done immediately after the preparation of the samples to avoid any visible α → δ phase transition. The fastest transition was visually observed for the as-prepared $FAPbI_3$ films crystallized at 80 °C and took 2 hours, but even in this case the XRD experiment proceeded faster. XRD patterns were fitted using the software TOPAS program using the Pawley method.

2.3 Temperature dependent measurements

Temperature-dependent Raman spectroscopy measurements were performed in a module THMS600 from Linkam Scientific. The chamber of the heating module was open during the measurements to avoid water condensation over the sample. $FAPbI_3$ was heated from 20 to 200 °C and measured in temperature steps of 30 °C, maintaining the selected temperature for 10 min for the sample to reach thermal equilibrium with the heating stage. After identifying a transition between 80 °C and 110 °C, additional measurements were done at 90 °C, 95 °C and 100 °C. PL measurements were performed in the same way, with temperature steps of 10 °C and an integration time of 1 s. Temperature-dependent XRD measurements were conducted in ambient air as described above using the high-temperature chamber TC-DOME with Be-walls from Anton Paar. XRD patterns were recorded for several selected temperatures in the range from 30 °C to 180 °C. Each pattern was recorded in a 2θ scan from 5° to 70° with a step size of 0.01° and an integration time of 1.2 s per step.

2.4 Methodology

The SCs remain in the as-synthesized state for less than 24 h in air after synthesizing, degrading heterogeneously. Within this time, the appearance of the $FAPbI_3$ samples became yellow by eye. The recovered samples were obtained by heating the degraded samples to 180 °C for 2 min on a hot plate and cooling down to RT.[7] The as-synthesized and the recovered samples were measured immediately after preparation and the degraded one after 24 h exposure in air. The spectra of the degraded samples were obtained using micro-Raman maps with a spacing of 5 μm to scope the heterogeneous surface. The preferable sample positions to measure the as-synthesized samples were located at the crystal borders or side planes, where the PL signal is lowered enough to disclose the low-frequency zone (<200 cm^{-1}).

3 Results and discussion

In this section, we describe and distinguish the structural polymorphism of $FAPbI_3$ at RT: 1 – as synthesized or initial α_i, 2 – degraded δ and α_δ, and 3 – thermally recovered α_{rec} and PbI_2. The alpha phase at high temperature is distinguished as α_{HT}. The attribution of the corresponding structures was supported by following the phase-transitions as presented in Table 1: (a) temperature-driven phase transition $\alpha_i \rightarrow \alpha_{HT}$, (b) time-driven phase transition $\alpha_i \rightarrow \alpha_\delta + \delta$, and (c) temperature-driven phase transition $\alpha_\delta + \delta \rightarrow \alpha_{HT} \rightarrow \alpha_{rec} + PbI_2$.

3.1 As synthesized α_i-$FAPbI_3$

Thin film α_i-samples are analyzed through XRD, with a mean value of the lattice constant of $a = 6.372$ Å considering the cubic $Pm\bar{3}m$ symmetry[12] (see Fig. S7, ESI†). As noted above, it is probably inconsistent to attribute to the α_i-structure the cubic $Pm\bar{3}m$ symmetry. In fact, states with different structural instability cannot possess the same structure. As agreed in the literature, the α_{HT}-phase, which is stable at 180 °C, has a primitive cubic cell. Furthermore, group theory dictates that cubic $Pm\bar{3}m$ Pb-based hybrid perovskites present only active Raman modes for low-coupled and strictly molecular vibrations,[21] which are over 200 cm^{-1} for FA^+. This is experimentally supported in the case of α-$MAPbI_3$.[2,22] Following this reasoning, we performed a thermal analysis of the sample from RT to 200 °C to identify the structural differences between the two boundary states. Temperature-dependent Raman spectra are shown in Fig. 1, while supporting PL and XRD measurements are presented in Fig. S5a and S6 (ESI†).

The Raman spectrum at RT shows the expected 4 Raman modes in the low frequency region: mode 1 – octahedral distortion (M1 at 43 cm^{-1}), mode 2 – molecular in-plane rotation around a corner H (M2 at 63 cm^{-1}), mode 3 – molecular out-of-plane rotation around the N–N axis (M3 at 96 cm^{-1}), and mode 4 – molecular translation (M4 at 114 cm^{-1}).[3] In the range from 20 °C to 100 °C, these 4 modes slightly broaden and red-shift. Beyond 100 °C only M4 remains, broadening and blue-shifting.

Table 1 Scheme of the phase-transitions: high temperature structure (α_{HT}), as-synthesized (α_i), thermally-recovered (α_{rec}), and degraded (α_δ). Secondary phases δ and PbI_2 are shown for clarification

	Variable	Initial state	Treatment	Final state
(a)	$T°$	α_i	20°C → 200°C	α_{HT}
(b)	Time	α_i	1 day	$\alpha_\delta + \delta$
(c)	$T°$	$\alpha_\delta + \delta$	20°C → 200°C → 20°C	$\alpha_{rec} + PbI_2$

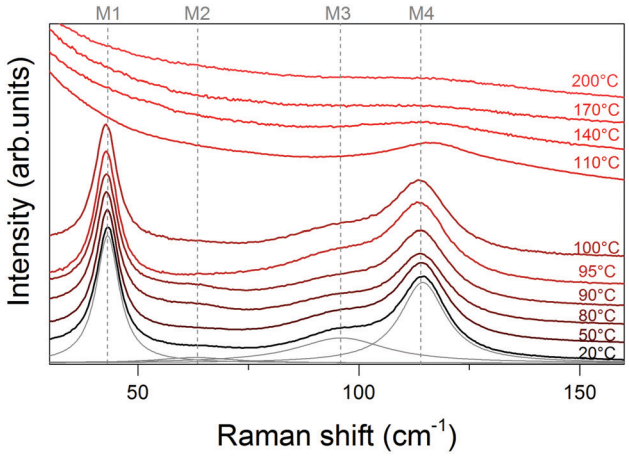

Fig. 1 Raman spectra of phase transition $\alpha_i \rightarrow \alpha_{HT}$ in $FAPbI_3$ in ambient air. Lorentzian-fitted Raman peaks for the RT spectrum are indicated by gray curves and identified at the top as MX, with $X \in [1,4]$.

A stepwise conjugated change of the full width at half maximum and Raman shift with temperature may indicate a phase transition in perovskites.[23] Thus, we deal with some structural reorganization in α_i-$FAPbI_3$ at 100–110 °C. Following the quantification of the temperature range for the phase transition from the α_i to the α_{HT} phase, we next focus on the properties of the $FAPbI_3$ structure before this transition.

Basically, phase transitions in perovskites can be caused by changes in the motion of the organic cation and its interaction with the lattice.[24,25] At temperatures below 100 °C, the I^- atoms displace within a characteristic time of 10 ps[19] and cannot rearrange as fast as FA^+ groups rotate (2 ps),[12] breaking the lattice centrosymmetry. This leads to the activation of Raman modes in the α_i-phase. At temperatures higher than 110 °C, the Raman modes are suppressed due to the spherical rotation of the FA cations and the faster response of I ions. If the molecule rotates spherically with almost statistical symmetry, the structure can be considered as centrosymmetric. This means that the vibrational modes do not change the polarizability of the structure at the equilibrium position of the ideal cubic perovskite. As a consequence, the Raman modes become inactive.[21,22]

The inactivation of modes in the thermally restructured α_{HT}-polymorph can be explained as follows. By definition, an asymmetric vibration in a symmetric system should be Raman inactive. This is the case of M1. In the case of M2 and M3, the center of charge is almost static: M2 constrains the vibration in

the plane where FA^+ is located, and in M3 the center of charge is kept within the rotation axis. M4 is the last remaining active mode after the transition since it involves the displacement of the molecular cation and consequentially I ions. Finally, this conjugated displacement results in a shift of the charge center. The mode gets broader when the amplitude of polarization reduces since the cation translation loses its preferential direction.

According to MD calculations, there is a weak anharmonicity of I^- displacement existing in $FAPbI_3$ below 97 °C, diverting the structure from the ideal configuration.[20] Several experimental details match this idea. These include the optimum temperature for single crystal growth in the range of 100–125 °C,[9] long-term stability of $FAPbI_3$ crystals at 87 °C inside the mother liquor[10] and the phase-transition of FAI into the cubic form at 113 °C.[26] In this work, we discovered a slope variation of the wavelength shift in the PL curve (Fig. S5a, ESI†). Along with this change, the lattice constant of $FAPbI_3$ shrinks on heating from 80 to 120 °C (Fig. S6 and Table S1, ESI†).

Therefore, it is clear that the structure α_i has highly displaced I^- atoms and low molecular rotation. As noticed above, MD calculations suggested for $FAPbI_3$ a cubic body centered cell with $Im\bar{3}$ symmetry at RT.[19] Our XRD investigation does not reveal any peak characteristic of this symmetry, for instance at 22.5° and 26.5° (see Fig. S7b, ESI†). However, modelling XRD patterns in the VESTA program discloses that this method is: (i) insensitive to the position and/or ordering of organic cations; and (ii) insensitive to the dynamics of the PbI_6-network if its average disposition remains the same. Therefore, the already known head-to-tail organization of the FA^+ molecules[10,18] associated with the I^- displacements at RT can be attributed to the difference between the α_i and α_{HT} phases observed in Raman/PL spectra.

To summarize, the as-prepared $FAPbI_3$ appears in a distorted cubic form with $Im\bar{3}$ symmetry due to the anharmonicity of iodine displacements. When heated up to 100–110 °C, it transforms into the ideal perovskite with $Pm\bar{3}m$ symmetry. At higher temperature, the active rotation of FA^+ ions results in geometrical sphericity, which provides higher crystal symmetry.

3.2 Degraded α_δ + δ-$FAPbI_3$

The yellow polymorph of $FAPbI_3$ is usually obtained at RT from the α_i-phase with time and remains stable for more than 10 weeks storage in a vacuum. This is a result of the structural instability of the α_i-phase due to internal stresses.[1] The analysis of the XRD patterns of degraded thin films reveals the coexistence of two phases: $Pm\bar{3}m$ (20.99%) and $P6_3mc$ (79.01%). The cubic phase presents a lattice constant of 6.361 Å (see Fig. S7 and S8, ESI†).

Visually yellow SCs demonstrate under the microscope three different zones: yellow needles, a dark matrix and an intermediate zone of small yellow round crystals of approx. 1 μm. We analyzed each zone using Raman spectroscopy (see Fig. 2).

The dark matrix (denoted as α_δ) presents a similar Raman spectrum to the α_i-phase. The main difference is a red-shift of 15 cm^{-1} of the Raman spectrum of α_δ compared to α_i. This is related to a variation of the Pb–I bond direction and consequentially a distortion of the unit cell. It is also visible in the blue shift of the PL signal, which has a wavelength around 100 nm shorter than the α_i-phase (see Fig. S2, ESI†).

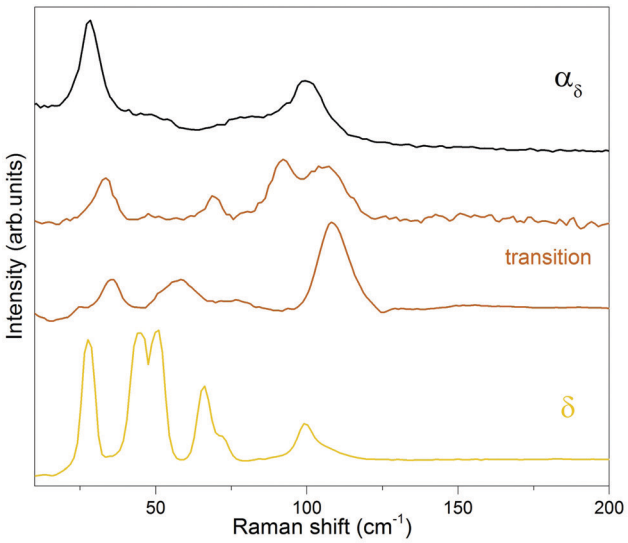

(a)

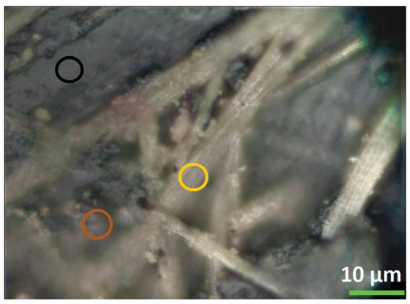

(b)

Fig. 2 (a) Raman spectra of the polymorphism of a degraded $FAPbI_3$ SC associated by color with the measurement point shown in (b) the microscope image (magnification ×10).

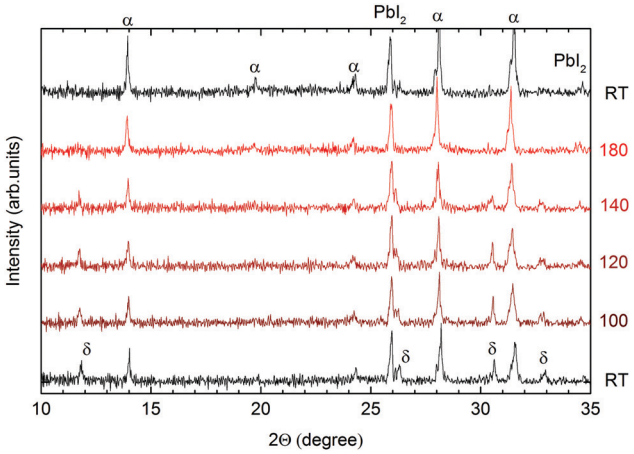

Fig. 3 Temperature dependent XRD analysis of degraded $FAPbI_3$ powder. The transition to the recovered state starts above 140 °C and finishes by 180 °C.

The small round yellow crystals show different Raman spectra, as presented in brown in Fig. 2. These spectra possess two distinctive qualities: a red-shift of M1 and M4 around 13 cm^{-1} with respect to the α_i-spectrum and sharpening and degeneration of M2 and M3. We identified these characteristics with the partial merging of the octahedra corresponding to the intermediate states of the transition $\alpha_i \rightarrow \delta$.

The yellow needles appear in the Raman spectrum as pure δ-phase. The Raman spectrum shows six peaks in the low-frequency range (<200 cm^{-1}). M1 and M4 are kept at the same position as α_δ, while M2 is split into two peaks at 44 and 51 cm^{-1}, and M3 into two peaks at 66 and 72 cm^{-1}. This variation from the α_i-spectrum coveys the structural change. In the case of the hexagonal $P6_3mc$ lattice, the octahedra merge in a 2-fold disposition and interconnect by faces along the ⟨001⟩ directions.[10] The red shift with respect to the α_i-spectrum is a consequence of longer Pb–I bonds. According to the XRD analysis on degraded thin films, the cell parameters of the hexagonal lattice are a = 8.682 Å and c = 7.929 Å. This means Pb–I bond lengths of 3.20 Å and 3.25 Å, longer than the 3.19 Å presented in the α_i thin films (see Fig. S7 and S8, ESI†). Additionally, two FA^+ ions of the elementary cell affect *via* molecular reorientation three double-merged octahedral units and *vice versa*. This results in the splitting and sharpening of coupled modes.

With the information from Raman spectroscopy, we can interpret the temporal transition α_i to δ as follows. Initially, the distortion of the $FAPbI_3$ cubic structure leads to the nucleation of the δ-phase at the most defective sites of the α_i-matrix. Then, some octahedra expand and merge together, encircling two organic cations per unit cell. This starts the growth of a second phase as different crystals. The octahedra continue merging in

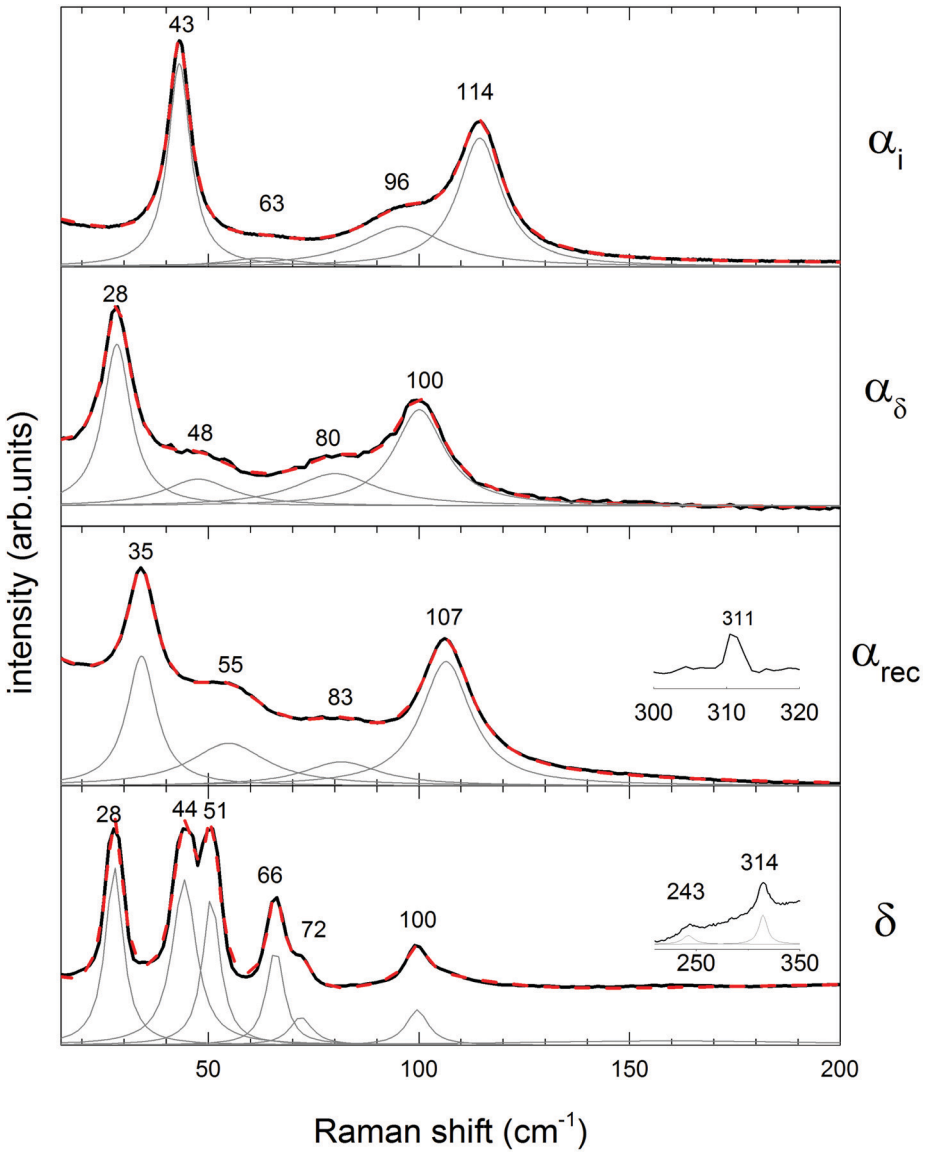

Fig. 4 Raman spectra of $FAPbI_3$ polymorphism acquired at RT. The black lines indicate experimental data, while the red dotted lines indicate the resulting fitted curves obtained from the superposition of Raman modes shown as Lorentzian-functions in gray.

the vicinities, leading to the consolidation of the hexagonal structure. Thus, the yellow needles of a pure δ-phase grow.

3.3 Thermally recovered α_{rec}-$FAPbI_3$ + PbI_2

The transition from degraded to recovered was followed by *in situ* powder XRD, as presented in Fig. 3.

The following changes can be noticed: the hexagonal lattice turns into a cubic one during heating from RT to 100 °C. Between 100 °C and 140 °C, the XRD patterns can be described by the superposition of two phases with hexagonal and cubic space groups. The main transition occurs between 140 °C and 180 °C, where the δ-phase fully disappears. This fact is supported in the literature by an endothermic peak around 160 °C detected by differential scanning calorimetry.[15] After cooling, the sample contains cubic $FAPbI_3$ (α_{rec}) and PbI_2. Recovered thin films show on average 25% of PbI_2 (see Fig. S7 and S8, ESI†). The presence of this non-photoactive PbI_2 works as superficial traps, decreasing the amplitude of the PL signal about tenfold as compared to α_i under the same illumination conditions.

A thermally recovered SC was analyzed by Raman spectroscopy and compared to the other polymorphs of $FAPbI_3$ at RT, as shown in Fig. 4. From an initial inspection, all polymorphs differ one from another.

The Raman spectrum of the α_{rec}-sample shows the same 4 modes of α_i with 3 distinctions: (i) a red-shift of 9 cm^{-1}, (ii) an increase in the intensity ratio between M2 and M3 from 0.22 (α_i) to 1.84 (α_{rec}), and (iii) the appearance of an additional mode at 311 cm^{-1}.

The first variation is analogous to the case of α_δ. The red-shift of the Raman spectrum suggests a weakening of the Pb–I bond, which is a consequence of a variation either in the bond length or angle. As extracted from our XRD on thin films, α_i and α_{rec} have similar lattice constants. Thus, a change of the Pb–I bond direction is involved. This distortion is lower than the one of α_δ, as evidenced by the lower magnitude of the red-shift and the lesser shift of the PL signal position (see Fig. S3, ESI†).

For the second change, different $FAPbI_3$ polymorphs at RT are compared in terms of the IM2/IM3 ratio and stability in Table 2. We can deduce a direct impact of the M3 relative intensity on the perovskite stability. This mode represents the out-of-plane rotation of FA^+ around the N–N axis and solely causes volumetric changes since all other modes are active in a molecular plane. The data on doped $Cs_{0.1}FA_{0.9}PbI_3$ and $Cs_{0.1}FA_{0.9}PbI_{2.6}Br_{0.4}$ compounds also support this finding.[3]

The third characteristic is the peak at 311 cm^{-1} of the α_{rec}-spectrum, which also appears in the δ-phase at 243 and 314 cm^{-1}. These correspond to the modes ''symmetric and asymmetric out-of-plane bending of FA^+''.[3] In the spectra of α_i and α_δ, the absence of this mode could be either veiled due to luminescence or inactive. In the last case, it may be the result of static hydrogen atoms, which govern these modes.

It is worth noticing that the transition temperature from α_{rec} to α_{HT} coincides with the transition α_i to α_{HT} according to the temperature dependant shift of the PL position (Fig. S5, ESI†).

It can be concluded that higher stability of the α_δ-phase in the degraded sample is interconnected with the constriction of volumetric displacement of FA^+. The latter is expressed as a hindering of the mode ''out-of-plane rotation around the N–N axis''. Both constituent phases, δ and α_δ, have similar density: 4.10 g cm^{-3} (ref. 10) and 4.00 g cm^{-3} (ref. 12), respectively. Moreover, the lattice constant in the SC remains almost unchanged in the α_i to α_δ transition, discarding the possibility of stress release.

The even higher stability of the α_{rec}-phase in the recovered sample can be explained by stress release, which is known to improve the stability of hybrid perovskites.[1] The observed expanded lattice of the α_{rec}-phase (see Fig. S9, ESI†) corresponds to release of isotropic compressive stress. This may be bound exactly with the formation of PbI_2, which is appreciably denser: 5.36 g cm^{-3}. In turn, lead iodide has the same structural fragments as the delta-phase (face shared PbI_6-octahedra), which gives rise to PbI_2 formation in a compressive environment during heating. Moreover, the fact that the mixture of the α_δ/δ phases undergoes a solid phase transformation causes multiphase interfaces facilitating nucleation of PbI_2. A remarkable suppression of the ''out-of-plane rotation around the N–N axis'' mode is also observed in the α_{rec}c-phase, becoming almost inactive as in the case of the isolated molecule. This points to a larger unoccupied volume for the free rotation of the molecule, uncoupling from the surrounding octahedra.

Table 2 Correlation between the $FAPbI_3$ phase stability in ambient air and intensity ratio of Raman modes M2 and M3. The spectrum and synthesis of α_δ are presented in Fig. S4 (ESI). The data on doped $FAPbI_3$ compounds are taken from our previous work.[3] The term ''stable'' considers the invariability of the Raman spectrum for more than 10 weeks

Phase	I_{M2}/I_{M3}	Stability
α_i	0.22	Unstable. 1 day
α_δ	0.83	Unstable. 7 days
α_{rec}	1.77	Unstable. 20–30 days[7]
α_δ*	8.98	Stable
$Cs_{0.1}FA_{0.9}PbI_3$	1.11	Unstable. 7 weeks
$Cs_{0.1}FA_{0.9}PbI_{2.6}Br_{0.4}$	2.67	Stable

4 Conclusions

We distinguished in our experiments three polymorphs of photo-active α-$FAPbI_3$ existing at RT: as-synthesized (α_i), degraded (α_δ) and thermally recovered (α_{rec}). They mostly differ in the level of distortion, the product of a secondary phase: δ for the degraded sample and PbI_2 for the thermally recovered one. The Raman spectrum of the α_i-phase points at the highest activity of the Raman mode ''molecular rotation around the N–N axis'', which is likely a main factor in the structural instability.

We proposed the α_i-$FAPbI_3$ crystals to have a cubic $Im\bar{3}$ structure at RT. Herewith, the FA^+ molecules are organized in a head-to-tail fashion and the displacement of I^- ions proceeds slower than the FA^+ displacement. Raman spectroscopy disclosed a transition of this distorted phase into the ideal

perovskite with $Pm\bar{3}m$ symmetry around 100–110 °C, where the corresponding Raman modes become inactive.

We demonstrated that the understanding of vibrational dynamics in hybrid perovskites could bring additional assets in the development of new and stable structures.

Conflicts of interest

There are no conflicts to declare.

Acknowledgements

The authors gratefully acknowledge the financial support provided by the Scholarship Becas Chile-DAAD 2017/91645541 and the German Federal Ministry for Economic Affairs and Energy (BMWi) under contract number 0324095H (speedCIGS).

Notes and references

1 X. Zheng, C. Wu, S. K. Jha, Z. Li, K. Zhu and S. Priya, *ACS Energy Lett.*, 2016, **1**, 1014–1020.
2 A. M. Leguy, A. R. Goñi, J. M. Frost, J. Skelton, F. Brivio, X. Rodrguez-Martnez, O. J. Weber, A. Pallipurath, M. I. Alonso and M. Campoy-Quiles, *et al.*, *Phys. Chem. Chem. Phys.*, 2016, **18**, 27051–27066.
3 J. Ibaceta-Jaña, R. Muydinov, P. Rosado, H. Mirhosseini, M. Chugh, O. Nazarenko, D. N. Dirin, D. Heinrich, M. R. Wagner and T. D. Kühne, *et al.*, *Phys. Chem. Chem. Phys.*, 2020, **22**, 5604–5614.
4 A. Kojima, K. Teshima, Y. Shirai and T. Miyasaka, *J. Am. Chem. Soc.*, 2009, **131**, 6050–6051.
5 S. Pang, H. Hu, J. Zhang, S. Lv, Y. Yu, F. Wei, T. Qin, H. Xu, Z. Liu and G. Cui, *Chem. Mater.*, 2014, **26**, 1485–1491.
6 N. Pellet, P. Gao, G. Gregori, T.-Y. Yang, M. K. Nazeeruddin, J. Maier and M. Graetzel, *Angew. Chem.*, 2014, **126**, 3215–3221.
7 Q. Han, S.-H. Bae, P. Sun, Y.-T. Hsieh, Y. Yang, Y. S. Rim, H. Zhao, Q. Chen, W. Shi and G. Li, *et al.*, *Adv. Mater.*, 2016, **28**, 2253–2258.
8 L. Ma, D. Guo, M. Li, C. Wang, Z. Zhou, X. Zhao, F. Zhang, Z. Ao and Z. Nie, *Chem. Mater.*, 2019, **31**, 8515–8522.
9 M. I. Saidaminov, A. L. Abdelhady, G. Maculan and O. M. Bakr, *Chem. Commun.*, 2015, **51**, 17658–17661.
10 C. C. Stoumpos, C. D. Malliakas and M. G. Kanatzidis, *Inorg. Chem.*, 2013, **52**, 9019–9038.
11 A. Binek, F. C. Hanusch, P. Docampo and T. Bein, *J. Phys. Chem. Lett.*, 2015, **6**, 1249–1253.
12 M. T. Weller, O. J. Weber, J. M. Frost and A. Walsh, *J. Phys. Chem. Lett.*, 2015, **6**, 3209–3212.
13 M. C. Gélvez-Rueda, N. Renaud and F. C. Grozema, *J. Phys. Chem. C*, 2017, **121**, 23392–23397.
14 Z. Li, M. Yang, J.-S. Park, S.-H. Wei, J. J. Berry and K. Zhu, *Chem. Mater.*, 2015, **28**, 284–292.
15 N. J. Jeon, J. H. Noh, W. S. Yang, Y. C. Kim, S. Ryu, J. Seo and S. I. Seok, *Nature*, 2015, **517**, 476.
16 D. H. Fabini, C. C. Stoumpos, G. Laurita, A. Kaltzoglou, A. G. Kontos, P. Falaras, M. G. Kanatzidis and R. Seshadri, *Angew. Chem., Int. Ed.*, 2016, **55**, 15392–15396.
17 D. P. McMeekin, G. Sadoughi, W. Rehman, G. E. Eperon, M. Saliba, M. T. Hoerantner, A. Haghighirad, N. Sakai, L. Korte and B. Rech, *et al.*, *Science*, 2016, **351**, 151–155.
18 A. Amat, E. Mosconi, E. Ronca, C. Quarti, P. Umari, M. K. Nazeeruddin, M. Graetzel and F. De Angelis, *Nano Lett.*, 2014, **14**, 3608–3616.
19 M. Carignano, Y. Saeed, S. A. Aravindh, I. S. Roqan, J. Even and C. Katan, *Phys. Chem. Chem. Phys.*, 2016, **18**, 27109–27118.
20 M. A. Carignano, S. A. Aravindh, I. S. Roqan, J. Even and C. Katan, *J. Phys. Chem. C*, 2017, **121**, 20729–20738.
21 A. Maalej, Y. Abid, A. Kallel, A. Daoud, A. Lautié and F. Romain, *Solid State Commun.*, 1997, **103**, 279–284.
22 O. Yaffe, Y. Guo, L. Z. Tan, D. A. Egger, T. Hull, C. C. Stoumpos, F. Zheng, T. F. Heinz, L. Kronik and M. G. Kanatzidis, *et al.*, *Phys. Rev. Lett.*, 2017, **118**, 136001.
23 K. Nakada, Y. Matsumoto, Y. Shimoi, K. Yamada and Y. Furukawa, *Molecules*, 2019, **24**, 626.
24 G. Chapuis, R. Kind and H. Arend, *Phys. Status Solidi A*, 1976, **36**, 285–295.
25 R. Kind, *Ferroelectrics*, 1980, **24**, 81–88.
26 A. A. Petrov, E. A. Goodilin, A. B. Tarasov, V. A. Lazarenko, P. V. Dorovatovskii and V. N. Khrustalev, *Acta Crystallogr., Sect. E: Crystallogr. Commun.*, 2017, **73**, 569–572.